Three-Dimensional Structure of a Membrane-Microtubule Complex

JOHN M. MURRAY
Department of Anatomy, School of Medicine, University of Pennsylvania, Philadelphia, Pennsylvania 19014

ABSTRACT The unicellular algae *Distigma proteus* contain a group of aligned microtubules associated with their cell membrane. The association is maintained in isolated membrane fragments. The membrane-microtubule complex also includes a crystalline array of membrane particles. The major peptide component of this array was identified by labeling whole cells with radioiodine. The entire complex of membrane, particles, and microtubules is sufficiently well ordered to permit reconstruction from electron micrographs by Fourier techniques. A three-dimensional model of the membrane array at a nominal resolution of 2.5 nm has been calculated. Some similarities were apparent between lattice spacings in the membrane array and in microtubules. Analysis of these lattice correlations suggests a way in which the array of membrane particles may serve as scaffolding for microtubule attachment.

A number of reports suggesting a link between microtubules and membrane-associated elements have been published (1–7). Unfortunately, these examples have not been suited for structural studies at higher resolution than the original observations by thin section electron microscopy. Association of microtubules with the cell membrane is a prominent feature of the cytoarchitecture of algae of the class Euglenophyceae (8–11). It is likely that the microtubules are involved in the dramatic shape changes known as euglenoid movement (8). The stability, predictable location, and highly organized arrangement of these membrane-bound microtubules makes them much more attractive for structural investigation than the previously described cases. In the hope of furthering our understanding of microtubule-membrane interactions in all cells, a structural and biochemical investigation of the specialized membrane-microtubule complexes from these algae has been undertaken. I report here the three-dimensional structure of the membrane microtubule complex from *Distigma proteus*. An investigation of the biochemical properties of this complex is being reported separately (12).

MATERIALS AND METHODS

Cell Culture and Preparation of Membrane Fragments: *Distigma proteus* was obtained initially from the Culture Center of Algae and Protozoa, (strain number CCAP 1216/3a; Cambridge, England) and later from the Culture Collection of Algae at the University of Texas at Austin, Texas (strain number UTEX 508). In both cases, cultures were maintained at room temperature on soil-water media (13).

Cells were harvested and washed several times with distilled water, using centrifugation at 600 *g*. Washed cells were resuspended in 0.1 M 2-(*N*-morpholino-ethanesulfonic acid (MES), 5 mM $MgCl_2$, 1 mM *p*-tosyl-L-arginine methyl ester (TAME), 0.1 mM phenylmethylsulfonyl fluoride (PMSF), 1 μg/ml pepstatin A, 1 mM EGTA pH 6.4 (henceforth buffer A) and then broken by brief low power sonication or by shaking with glass beads. Membrane fragments were collected and washed in buffer A by centrifugation at 3,000 *g* and used immediately for structural studies.

For analysis of peptide composition by gels, further purification was necessary. Washing the cell membrane fragments in buffer A plus 0.2% NP-40 removed membranous remnants of other cell organelles selectively, since this membrane-microtubule complex is resistant to low concentration of nonionic detergents. Other particulate contaminants were removed by sedimentation to equilibrium in a density gradient of metrizamide. The membrane fragments were removed from the gradient, dispersed, and washed in buffer A, then sedimented to equilibrium in a second, continuous, metrizamide density gradient. The fragments formed a diffuse band at a density of 1.26. This fraction appears identical to that used for structural studies, as viewed by electron microscopy, except for a variable decrease in the number of microtubules remaining attached to the membrane.

Electron Microscopy: Samples were prepared for routine thin sectioning by fixation with 2.5% glutaraldehyde in the buffer used for cell breakage for 30 min, postfixing with 0.5% OsO_4 in 0.1 M $NaPO_4$ pH 6.0 on ice for 30 min, dehydration in a graded series of ethanol, then exchanging into propylene oxide prior to embedding in Spurr's (14) resin. For visualization of microtubule protofilaments, the modification by Binder and Rosenbaum (15) of Mizuhira and Futaesaku's (16, 17) original tannic acid protocol was followed exactly. Silver sections were cut with a diamond knife and stained with either 5% uranyl acetate for 30 min at 50°C, or 2% uranyl acetate in 2% methanol at room temperature for 10 min. In both cases, the sections were then further stained with lead citrate and examined at 80 kV in a Phillips EM 201 or EM 400, or at 150 kV in a JEOL JEM200A.

For scanning electron microscopy, washed cells were put in a thin layer on a carbon coated grid and plunged rapidly into a bath of propane at the temperature of liquid nitrogen. The frozen cells were transferred without warming into vacuum and lyophilized before sputter coating with gold-palla-

THE JOURNAL OF CELL BIOLOGY · VOLUME 98 JANUARY 1983 283–295

dium. The grid was then mounted over a hole in a sample stub and examined in an AMR 1000.

Membrane fragments were negatively stained with 2% uranyl acetate on thin carbon films and examined in a Phillips EM 400 at 80 kV using a 30-μ objective aperture. Micrographs were taken at a magnification of 19,500 or 25,000 using minimal dose techniques to keep the total electron exposure as low as possible. Samples were tilted in the microscope by means of the goniometer stage to ±60°, and beyond this by bending the grid before mounting it on the specimen injector rod.

Image Processing: The techniques used here for reconstructing an object in three dimensions from a two dimensional array closely follow those described by Unwin and Henderson (18, 19). Properly exposed micrographs free of drift and astigmatism and which were optimally underfocused (~900 nm) were considered for processing. Initial screening was carried out using a laser diffractometer to search for sufficiently large well ordered fragments of membrane. Promising areas were marked by placing small spots along their boundary. Digitization was carried out on a Perkin Elmer Model 1010 A scanning microdensitometer using a step size of 17 μm, a square aperture of 16.7 μm side, and recording optical density with a photometric resolution of 0.01 OD. The digitized images were displayed to determine coordinates for the boundary positions marked earlier. The selected areas were extracted from the scan and Fourier transformed, then displayed as plots of logarithm of the amplitude of the Fourier transform vs. spatial frequency for preliminary indexing of the reciprocal space lattice. Exact coordinates of the center of all strong spots were determined and used to find a set of least squares best lattice constants. Amplitudes and phases surrounding each point of the refined lattice were printed and examined for the presence of a reliable spot. A "reliable" spot was empirically defined as one that satisfied all of the following conditions. (*a*) The amplitude at the calculated lattice position, or neighboring grid point for nonintegral coordinates, was the highest value in a surrounding 9 × 9 array. (*b*) An obvious phase plateau occurred at the calculated lattice position. (*c*) No evidence of splitting of the spot into two regions of different phase or unsymmetrical smearing in any direction was seen. In practice, image defects are readily apparent since they degrade many reflections in the same way, allowing one to identify quickly images of poor quality. Comparison of many images established a set of reflections that were consistently present. Amplitudes and phases were taken from the exact positions of the calculated lattice point of this set of reflections, interpolating as necessary to find precise values when the calculated lattice position did not fall exactly on a transform grid point. Dimensions of the transform were usually chosen about twofold larger than the array of image densities, (typically 512 × 512) so that reflections were spread over several transform grid points, and minimal error was introduced by mismatch of transform grid points with reciprocal lattice positions.

Reflections from a set of micrographs at different tilt angles were refined to a common phase origin and plotted along each lattice line against spatial freuency in the direction perpendicular to the plane of the membrane (Z^*). Interpolation from these plots at equal intervals in Z^* for each reflection gave a set of Fourier coefficients on a regular three dimensional lattice, which were then used for calculating the final reconstruction.

The computer programs for calculating the Fourier transform were adapted from the system developed at the MRC (Medical Research Council) Laboratory of Molecular Biology, Cambridge, England, kindly provided by Dr. L. Amos. Some of the image and transform display routines were provided by Dr. D. Grano of the Structural Biology Department, Stanford University.

^{125}I-Surface Labeling and Gel Electrophoresis: The external surface of the membrane was labeled with ^{125}I by two different procedures. Cells were freed of debris, and deflagellated, by washing six times in distilled water. Lactoperoxidase catalysed iodination was carried out as described by Morrison (20) for 2 min on whole cells, which were then washed free of enzyme and substrates in buffer containing cold iodide. Alternatively, the cells were labeled by exposing them for 2 min at 0°C to the diazonium salt of [^{125}I]-iodosulfanilic acid (New England Nuclear Inc., Boston, MA). After either labeling method, cells were broken by sonication, and all particulate material collected by centrifugation at 5,000 *g* for 5 min. Labeled material in this pellet was analyzed by SDS gel electrophoresis followed by autoradiography. Electrophoresis in the presence of SDS was carried out using the buffer system of Laemmli (21). For silver staining, we followed the procedure of Bürk et al. (22).

RESULTS

Cell Morphology and Euglenoid Movement

Distigma proteus is a typical member of the class Euglenophyceae of flagellated unicellular algae (9). At rest, the cell is rod shaped, 50–60 μm long, 5–8 μm diam, with one end slightly tapered and the other rounded. This particular species is quite active in the characteristic contractions ("euglenoid" movement) exhibited in varying degree by many members of the class. A scanning electron micrograph of cells that were rapidly frozen during active shape changes is shown in Fig. 1. Transitions between the most dissimilar shapes present in Fig. 1 occur in ~1 s.

The cell surface is folded into longitudinal ridges, usually 18 in number, which trace a helical path along the length of the cell. These ridges, as seen in Fig. 1, are a permanent feature, changing in orientation with respect to the cell axis, but retaining a more or less constant profile through all the gross changes in overall cell shape. The contour of the ridges is presumably imposed on the membrane lipid bilayer by the

FIGURE 1 Scanning electron micrograph of *Distigma proteus*, trapped in various different shapes by rapid freezing. Folds in the cell membrane following a left-handed helical path along the cell are visible. Bar, 10 μm. × 2,400.

electron dense material apposed to its inner and outer surfaces. The two surfaces appear slightly different in thin sections (Fig. 2, *b* and *c*). The inner surface has a somewhat thicker, more intensely stained, and more uniform layer of material underlying it than is seen overlying the outer membrane surface.

Underlying every ridge are microtubules in three separate locations on the cytoplasmic surface (Fig. 2*b*). The largest group (*1* in Fig. 2*b*) lies on the smoothly curved border of each ridge. The number of microtubules at this location varies; as few as four and as many as nine have been observed. At the point where the membrane folds inward and makes a sharp bend, another group of two microtubules are found (*2* in Fig. 2*b*). The more peripherally located member of the pair is frequently an incomplete microtubule, and usually has a small arc of what appear to be tubulin protofilaments (Fig. 2*c*) attached at one point. This arrangement is similar to the structures induced in vitro when tubulin is polymerized in certain conditions. If it is the same arrangement of tubulin, then it is a guide to the polarity of the microtubule as shown by Heidemann and McIntosh (23). In this case, it would indicate that the more rapidly growing end of the microtubule (in vitro) is at the end of the cell distal to the flagella.

At the third location, beneath the deepest part of the surface groove, one or occasionally two microtubules were found. In Fig. 2*b*, the microtubules of the second and third group are close together, so that the distinction between them may appear somewhat arbitrary. In comparing many such sections however, it was found that whereas the location of the pair of microtubules labeled *2* is quite constant relative to the sharp bend in the membrane, the location of microtubule(s) *3* is more variable. It is on this basis that they have been distinguished. Of the three groups of microtubules, the largest cluster has been studied first structurally since it is easily visualized in negatively stained membrane fragments.

The microtubules are separated from the membrane lipid bilayer by a distance of ~12 nm. The intervening space may appear nearly empty, or be filled with an amorphous darkly stained material, depending on the method of fixation and use of tannic acid. In tannic acid treated cells, microtubule group *2* is embedded in the amorphous dark staining layer of material, which seems to continue as a thinner layer under the remainder of the membrane. Cells not treated with tannic acid show a much thinner layer of material underneath the lipid bilayer, and frequently show only tenuous connection between microtubules and the inner membrane surface.

Components of the Membrane-Microtubule Complex

Mechanical rupture of *Distigma proteus* yielded large pieces of the assembly of cell membrane, microtubules, and associ-

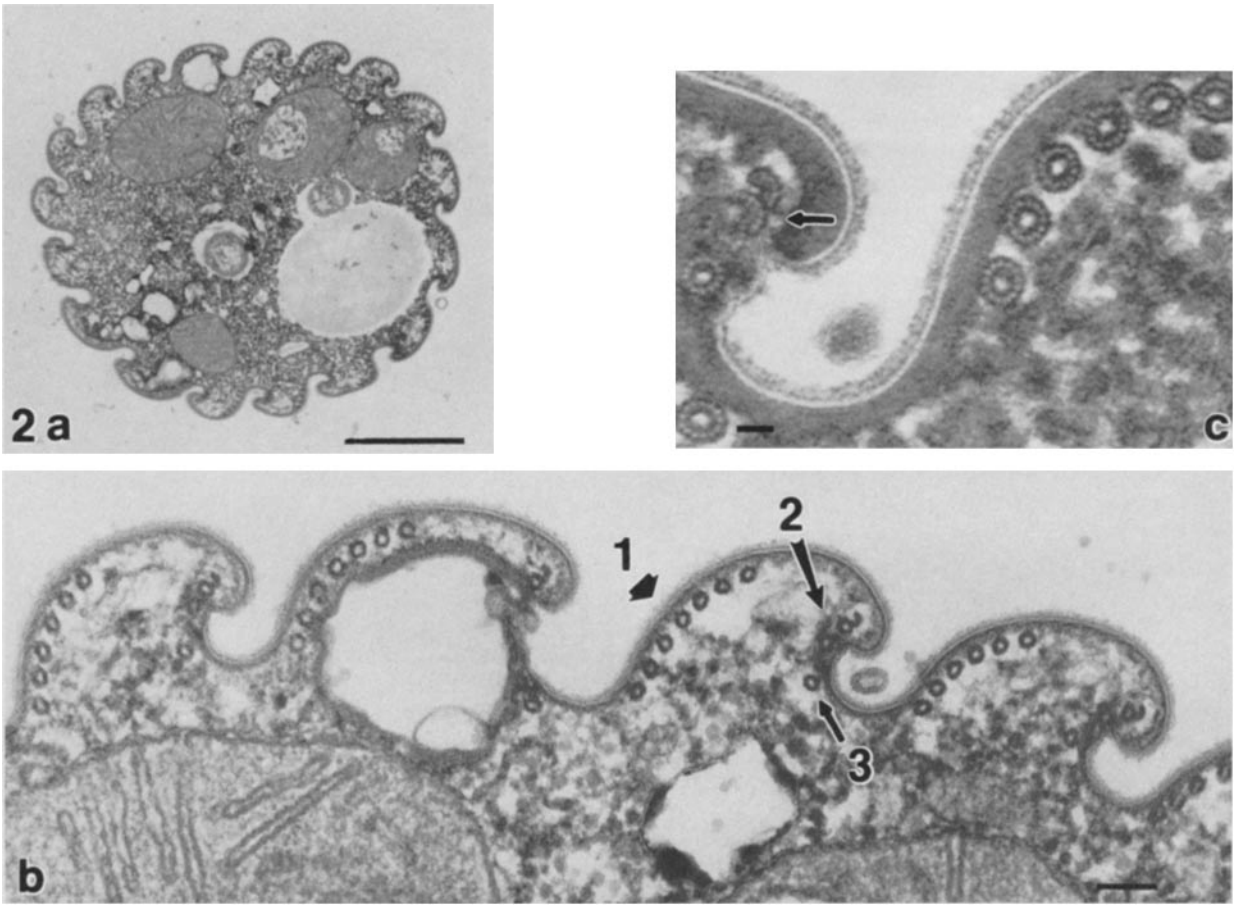

FIGURE 2 Section of *Distigma proteus*.The plane of section is approximately perpendicular to the long axis of the cell. (*a*) Low magnification view of the whole cell showing the 18 membrane folds. Bar, 1 μm. × 16,500. (*b*) Higher magnification view of the same cell, showing the three locations at which microtubules are found beneath every membrane fold. Bar, 100 nm. × 84,000. (*c*) Section of a cell fixed in the presence of tannic acid to show microtubule protofilaments. Each complete microtubule has 13 protofilaments. The arrow indicates a microtubule that usually bears an arc shaped appendage of what appear to be microtubule protofilaments. Bar, 20 nm. × 218,000.

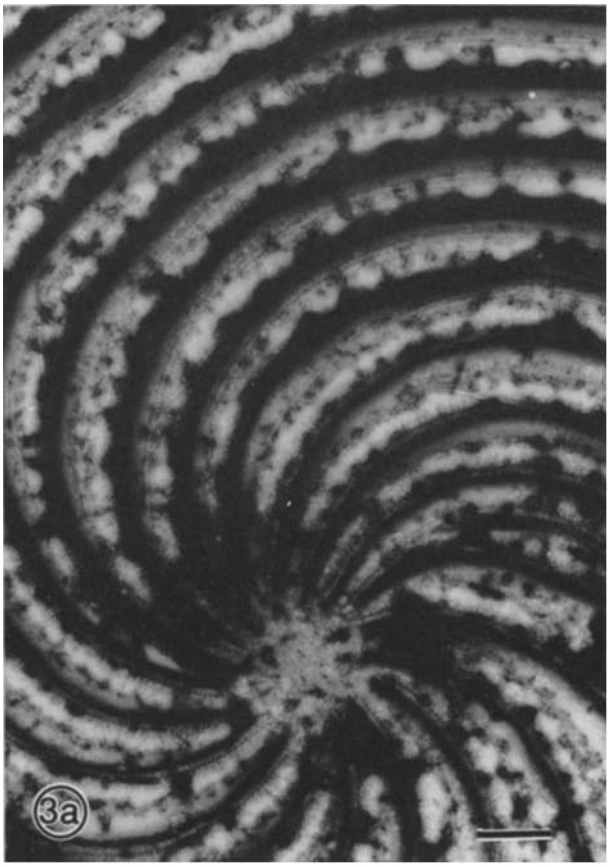
3a

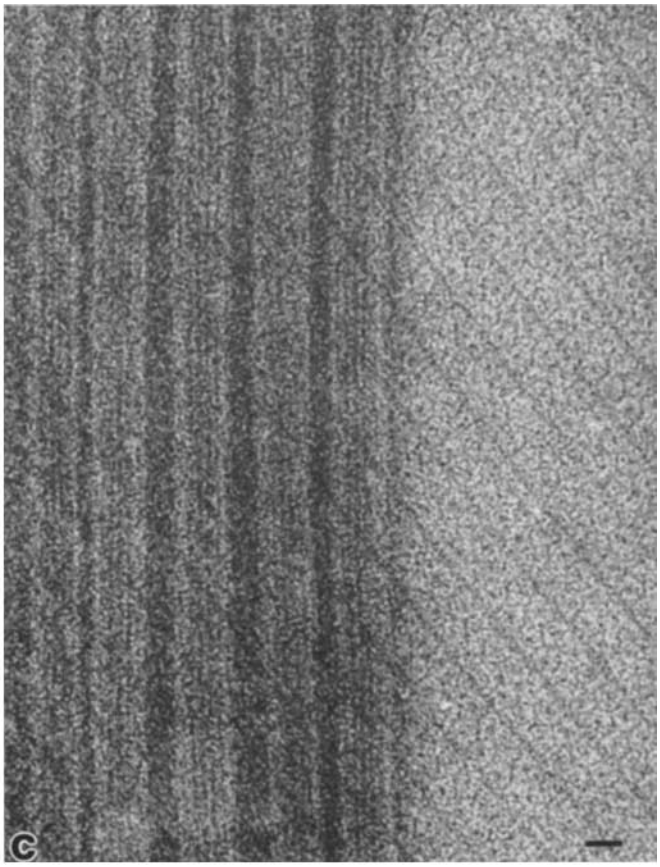
c

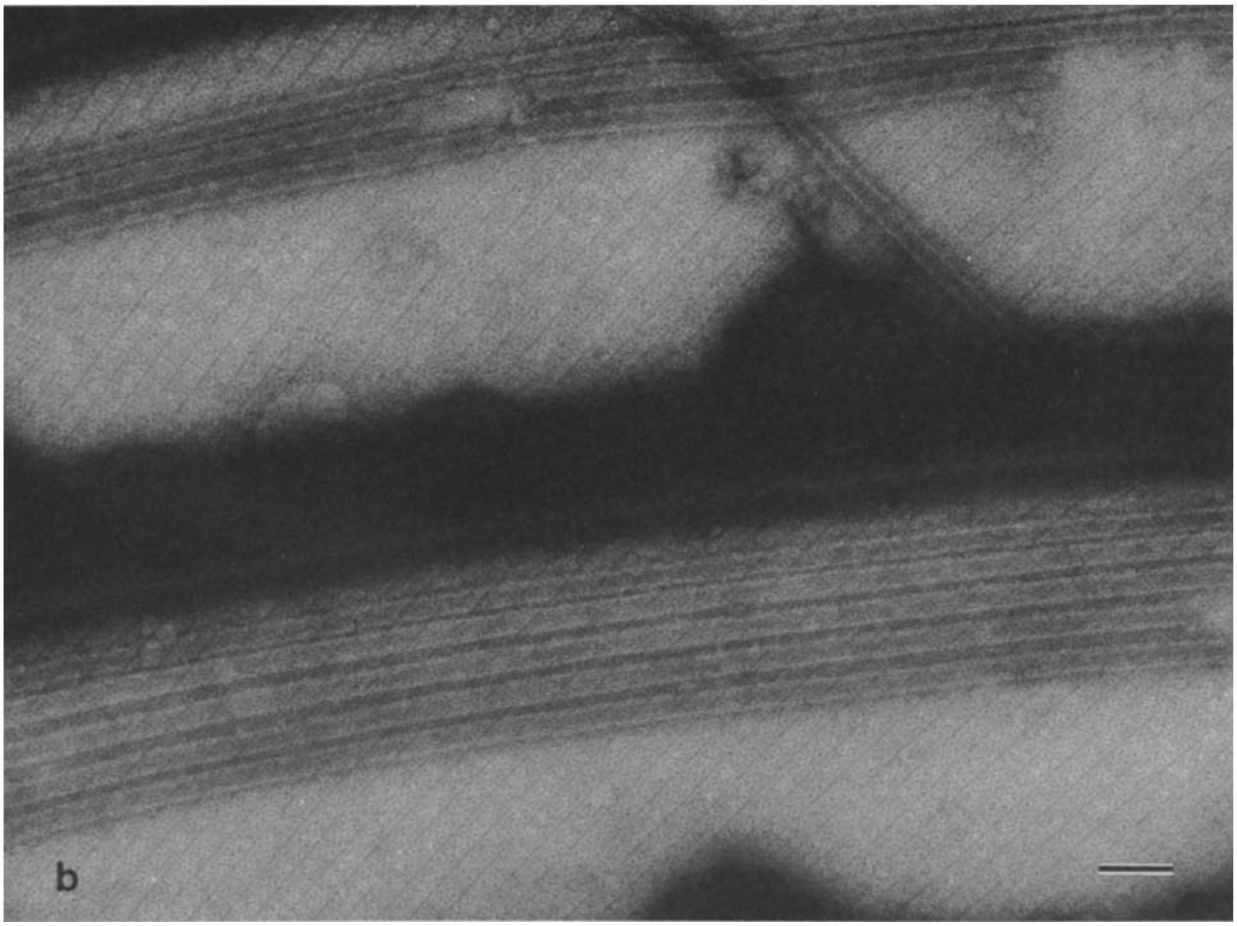
b

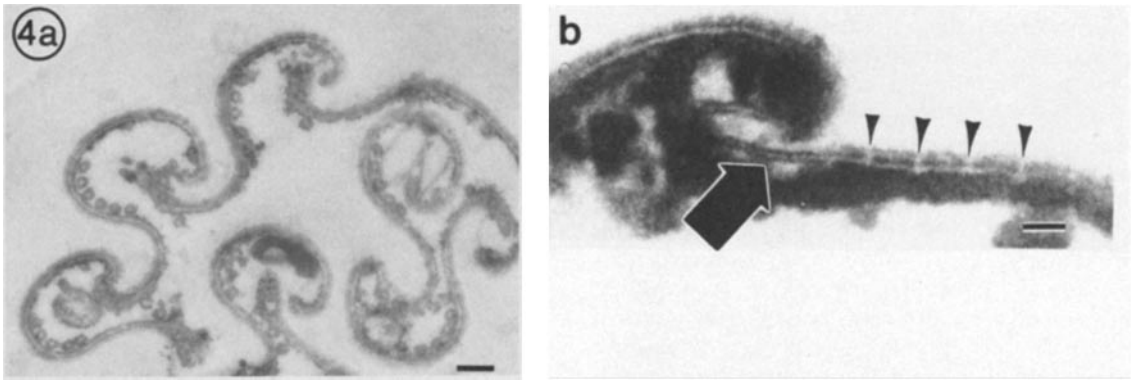

FIGURE 4 (a) Thin section of an isolated fragment of cell membrane. The membrane folds retain their characteristic shape and most of the microtubules remain attached after isolation. Bar, 100 nm. × 52,000. (*b*) An area oriented to show the borders between rows of membrane particles (arrowheads). The large arrow points to the strip of bare membrane located at the bottom of the groove between each membrane fold. Bar, 20 nm. × 260,000.

ated electron dense material. These pieces of membrane are sometimes sufficiently flat to give a useful image after negative staining. Fig. 3*a* shows a large piece of membrane lying flat on a carbon support film and after negative staining. This fragment includes the posterior (nonflagellated) end of the cell, where the folds of the cell surface terminate in a vortex. The membrane is incompletely flattened, and stain accumulation in the residual grooves gives the characteristic pattern of a very dark line bordering each more lightly stained membrane ridge. Most of the microtubules seen in thin sections of intact cells remain attached to the isolated membrane fragments (Fig. 4*a*). The group of microtubules labeled *1* in Fig. 2*b* is particularly well seen in negatively stained membrane fragments (Fig. 3*b*).

From observations of negatively stained whole cell "ghosts" and large fragments of membrane, it seems likely that the microtubules normally extend the length of the cell. However, when more vigorous breaking of the cells was done to obtain a higher yield of smaller fragments useful for structural studies, many microtubules were broken and sheared off the complex. The center to center spacing of adjacent microtubules, in thin sections of whole cells and negatively stained membrane fragments, varies from ~27 to 60 nm if many pairs of microtubules are examined. The distance between the members of any one pair is however much more constant, as the microtubules lie parallel to each other over long distances (Fig. 3*b*). Deviations from this parallel arrangement seen in Fig. 3*b* are believed to be the result of disruptive forces during cell breakage and negative staining of membrane fragments.

In addition to the microtubules, negative staining revealed a crystalline array of particles in the membrane. The particles are arranged into rows whose borders are visible as faint stripes tilted to the right of the vertical direction in Fig. 3*b*. The rows of particles cross the surface folds at an angle of ~35°. The particles are packed tightly in the array so that stain penetration is rather poor. Over most of the membrane, the limited penetration of stain does not give high enough contrast to permit visual definition of the borders of individual particles. In areas where the array is disordered, stain penetration is much better however, and individual particles can be distinguished. As the membrane dried down on the grid, incompletely flattened areas are the most severely distorted, hence better stained and thus appeared at first glance much better preserved than undistorted areas. This effect can be seen in Fig. 3*b* by carefully examining the area just to the left of the top center of the micrograph. In this area it can be seen that each row is two particles wide.

The dark bands of stain in the residual grooves obscures the underlying membrane in Fig. 3*b*. In occasional more flattened and lightly stained specimens, this area can also be seen, and it too is found to be covered almost completely by the same ordered array of particles. These particles normally cover all of the cell surface except for a narrow strip along each groove adjacent to the sharp bend in the membrane.

The rows of membrane particles are also seen in appropriately oriented thin sections of isolated membrane fragments (Fig. 4*b*). Here they appear to form a thin layer intimately associated with the extracellular surface of the lipid bilayer. The narrow strip of membrane free of particles is also indicated in Fig. 4*b*. Mechanical rupture of the cells, as well as detergent-induced lysis, predominantly splits the cell longitudinally along these bare strips. The membrane particles thus probably contribute significantly to the resistance of these cells to mechanical disruption. Their appearance in thin sections suggests that the particles are inserted into the membrane lipid bilayer, and thus are probably integral membrane proteins. An array of integral membrane particles has been seen

FIGURE 3 (a) Negatively stained fragment of isolated cell membrane. This portion includes the end of the cell opposite the flagella.The dark spiral stripes result from stain accumulation in the incompletely flattened membrane folds. Bar, 500 nm. × 20,000. (*b*) Higher magnification view of another negatively stained membrane fragment. The dark band running horizontally across the middle is a stain-filled groove separating two membrane folds. Most microtubules remain attached but a few are broken and displaced. Oblique striations demarcate the rows of a crystalline membrane lattice. Bar, 50 nm. × 220,000. (c) A well-ordered area of membrane-microtubule complex used for Fourier reconstruction. There are five nearly parallel microtubules crossing the rows of membrane particles at an angle of ~35°. The view in this as well as *a* and *b* is from the inside of the cell. Bar, 20 nm. × 246,000.

in freeze fracture studies of *Euglena gracilis*, another algae of the Euglenophyceae class (24, 25). The particles in that species are smaller and have a different shape than the ones seen in *Distigma*, but it is interesting to note that they too occur in rows that cross the surface folds at ~35°.

The biochemical properties of the membrane particle array were consistent with their identification as integral membrane proteins. The particles remained associated with the membrane and the array retained its order through repeated washes with water or buffers of pH 4-9 and ionic strength up to 1 M. (Extremes of pH and salt caused the membranes to roll up into a tightly wound spiral or other disordered aggregates in which the particle array can no longer be seen by negative staining.) Washing with mild nonionic detergents and chelating agents also failed to dissociate the particle array from the membrane. Therefore the particles are unlikely to be bound by primarily ionic bonds to the membrane complex. Strong detergents such as SDS or deoxycholate destroyed the membrane complex, and in the presence of sulfhydryl reducing agents dissolved it completely. Thus, the particle array is held together and bound to the membrane by strong hydrophobic interactions, and the complex as a whole is stabilized by disulfide bonds.

The extracellular portion of the particles is quite resistant to proteolysis, as might be expected for an organism that swims continuously in a dense culture of mixed soil bacteria and associated exoproteases. Brief treatments of membrane fragments with protease K or papain did not affect grossly the negatively stained appearance of the particle. Vigorous treatment (0.5 mg/ml for 1 h at room temperature) destroyed the ordered appearance of the membrane complex, leaving rolled up fragments and amorphous aggregates of material.

Membrane fragments, isolated as described in Materials and Methods and further purified by density gradient centrifugations resulted in the SDS gel electrophoresis pattern shown in Fig. 5*a*. ^{125}I-labeling of intact cells incorporated radioactivity mainly into a single peptide of high apparent molecular weight (Fig. 5*b*).

This band is a major component in silver or Coomassie stained gels of membrane complex and is therefore tentatively identified as a protein making up the particle array. Its molecular weight cannot be accurately estimated at present, since it migrated only ~1 mm into the separating gel. Control experiments (data not shown) showed that the labeled material in solution in SDS remained mostly in the supernatant after centrifugation at 93,000 *g* for 1 h, and that it was destroyed by protease treatment.

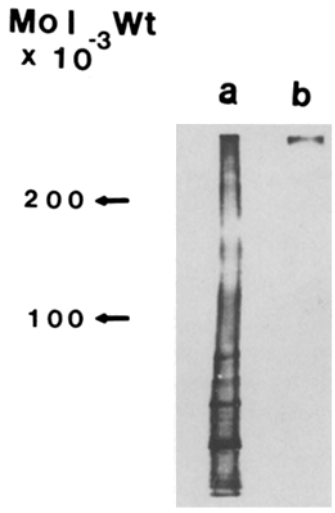

FIGURE 5 SDS gel electrophoresis of isolated membrane complex (*a*) stained for protein by the silver method. (*b*) Autoradiograph of a gel from intact cells labeled by extracellular treatment with diazotized [^{125}I]iodosulfanilic acid.

Three-Dimensional Reconstruction of the Membrane-Microtubule Complex

The regularly repeating arrangement of the membrane particles and microtubule cluster suggested that structural analysis to higher resolution and in three dimensions might be possible using Fourier transform based averaging methods as described by Klug and DeRosier (26). The success of this technique is partially determined by the extent of coherently ordered array available. The incomplete flattening of the surface folds limits the width of ordered array to less than the width of one surface fold. In the orthogonal direction, the length of coherently ordered array is limited by spiralling curvature of the folds in the plane of the membrane, i.e., the remnants of their once helical path along the cell. In addition to these small gradual but cumulative types of loss of coherence, the particles in the array also frequently show a more obvious type of sharply bounded dislocation. The latter defect is quite interesting in that it suggests how this apparently crystalline and, one would have supposed, rigid, array of particles is compatible with the observed rapid, fluid, deformations of the cell membrane during euglenoid movement. Careful examination of negatively stained membrane reveals that each row of the membrane array is two particles wide, and that each of these double rows of particles is staggered, by one-half of a particle width, with respect to neighboring double rows. Over large areas of membrane this alignment is precisely maintained. However, dislocations occur that disturb this alignment between double rows, yet leave undisturbed the relative locations of particles within a double row. In other words, sliding of the double rows past each other is occurring, and with a relatively low energy barrier judging from the frequency of this type of disorder. The cell membrane thus gains the mechanical strength of the layer of close packed membrane particles, yet retains flexibility with this relatively easy sliding of rows.

Although these various lattice distortions limited the coherent patches of array to much smaller areas than one might have hoped, sufficiently large ordered regions can nevertheless be found to make averaging techniques worthwhile. The diffraction pattern of the best preserved membrane fragments show reflections out to a resolution of ~2.4 nm, i.e., to near the limitations of the negative staining procedure.

The computed Fourier transform from a digitized micrograph of negatively stained membrane is shown in Fig. 6*a*. Diffraction spots from the surface array indicate a nearly orthogonal unit cell of dimensions 28 by 14 nm. (γ = 95°). Reflections extending out to the (10 3) are seen in the best preserved specimens.

Diffraction from the microtubules occurs on lines at an angle of ~35° counter-clockwise from the [1 0] direction of the lattice pattern. Instead of the usual lines of density expected from a single microtubule, the layer lines and equator in this pattern are rows of discrete spots. The layer lines are being "sampled" by a lattice spacing, since the microtubule diffraction pattern here arose from multiple regularly spaced microtubules. The particular area of membrane used for calculating Fig. 6*a* was chosen because its microtubules were all separated from each other by a nearly constant distance. Sampling of both the layer lines and equator indicates the

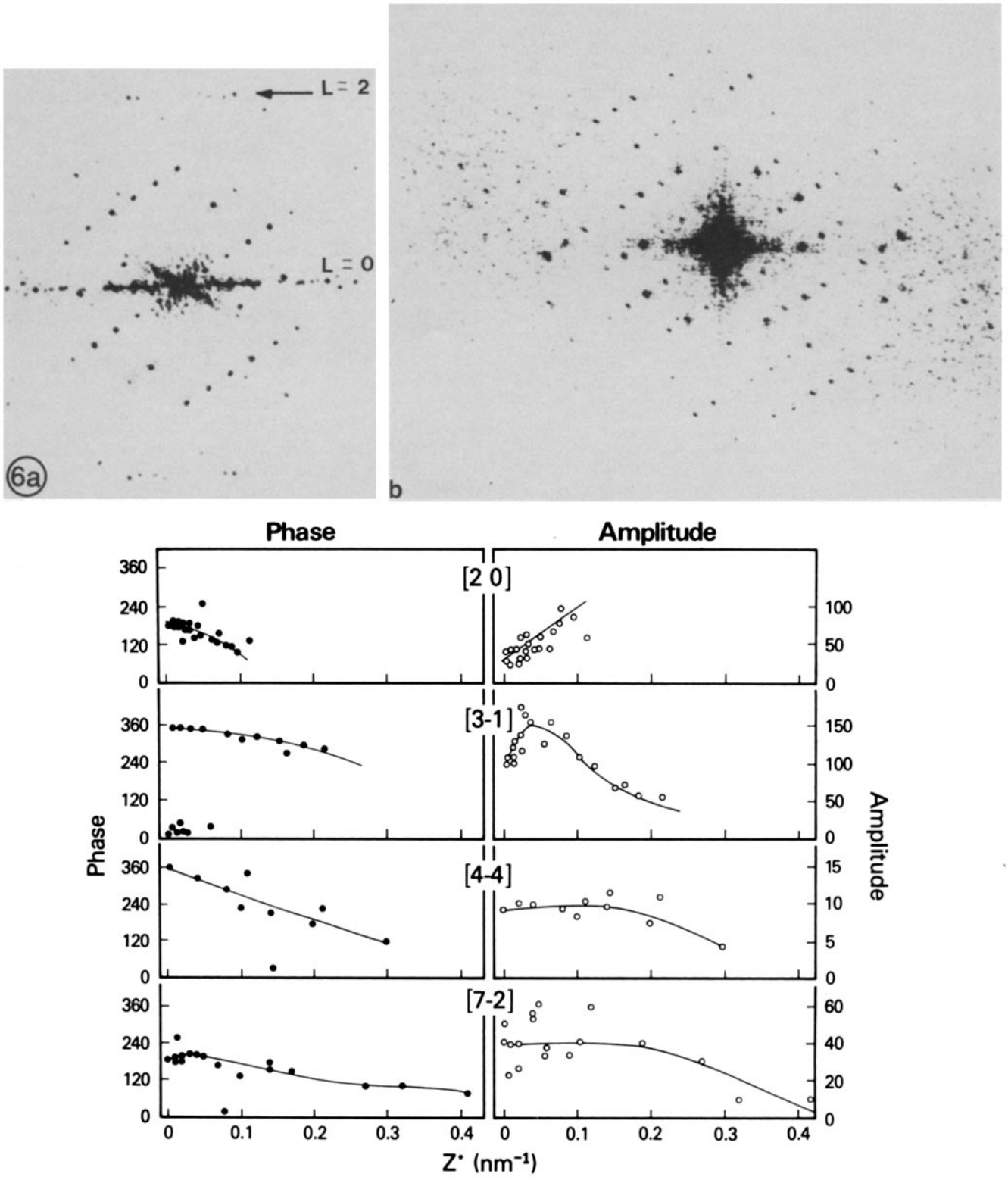

FIGURE 6 (*a*) Display on a logarithmic gray scale of the intensity of a computed Fourier transform of a digitized electron micrograph of a fragment of negatively stained membrane microtubule complex. The lattice has dimensions a = 27.9 nm, *b* = 14.3 nm, $\gamma = 95°$. The orientation is the same as Fig. 3*c*. The equator ($L = 0$) and ¼ nm^{-1} layer line ($L = 2$) of the microtubule pattern are indicated. (*b*) Computed Fourier transform intensity from an area of membrane lacking microtubules. Same orientation as *a*. (*c*) Amplitude and phase of four representative reflections of the membrane lattice plotted versus distance in reciprocal space perpendicular to the membrane (Z^*). Data points are taken from the Fourier transforms of micrographs of specimens tilted in the microscope. The continuous lines were drawn by hand.

adjacent microtubules have a more or less constant axial displacement with respect to each other as well as a constant lateral separation. The alternative arrangement, (i.e., parallel microtubules, constant lateral separation, but randomly shifted along their axis) would give sampling on the equator but an unsampled intensity distribution along the layer line. The position of each microtubule is thus not independent of its neighbors; rather, all are fixed relative to some common coordinate system. A likely candidate is of course the array of particles embedded in the membrane.

At several points in reciprocal space, the diffracted intensity from the microtubules merge with spots arising from the membrane particles. Thus the (3 $\bar{1}$) membrane spot lies very close to the microtubule equator, the (1 2) and (4 1) spots partly overlap the ⅛ nm^{-1} layer line, and the (6 3) and (5 3) partly overlap the ¼ nm^{-1} layer line. The pattern arising from membrane particles alone can be obtained by selecting an area of surface free of microtubules, as was done for Fig. 6*b*. Comparison of amplitudes and phases of the spots in Fig. 6*b* with the corresponding spots in Fig. 6*a* which are not affected by overlaps with the microtubule pattern reveals no significant differences. In addition, both data sets possess the symmetry (in projection) of the two-sided plane group p21 to within an average phase residual of 15°. Thus, at the current resolution (~2.5 nm) the average shape in projection of membrane array overlying microtubules is probably indistinguishable from that in microtubule-free areas. This simplifies the task of reconstructing the entire assembly in three-dimensions. It is difficult to achieve optimum staining while preserving order in the microtubule array because the microtubule-membrane linkage is quite sensitive to pH and ionic composition of the medium (12). Thus the rather extreme conditions (pH 4.5 or less, ionic strength 0.2 M or more) encountered during negative staining with uranyl acetate frequently dislodge the microtubules, necessitating some compromise between optimum staining and preservation of structure. This constraint does not however limit staining of the membrane particles alone, and they can be imaged at higher resolution, as seen by comparing Fig. 6, *a* and *b*. Membrane free of microtubules was therefore used to reconstruct the particle array in three-dimensions.

Micrographs of the membrane array were collected at various tilt angles up to 76°, and around two different tilt axes. These images were digitized and Fourier transformed, then phases and amplitudes were extracted at all reciprocal lattice points. Amplitudes not significantly above background noise were set to zero. The collected spots (~1,400 in all) were converted to a common amplitude scale and phase origin, then plotted individually along each reciprocal lattice line perpendicular to the plane of the membrane, as shown for a few representative lattice lines in Fig. 6*c*. These plots enabled the construction of a grid of evenly spaced samples of the three-dimensional Fourier transform of an average unit cell, within the sphere of limiting resolution of the data (except, of course, for the small volume inaccessible because of the limitations of tilt angles to <90°). A reconstruction of the original density distribution for an average unit cell of the membrane lattice was calculated (26) and used to make the model shown in Fig. 7, *a* and *b*. In interpreting this model, some limitations of the three-dimensional reconstruction technique must be kept in mind. Tilt angles in the microscope are limited to <90°, which means the final resolution perpendicular to the membrane will be less than in other directions. In addition, the (0 0) lattice line is not included in the Fourier

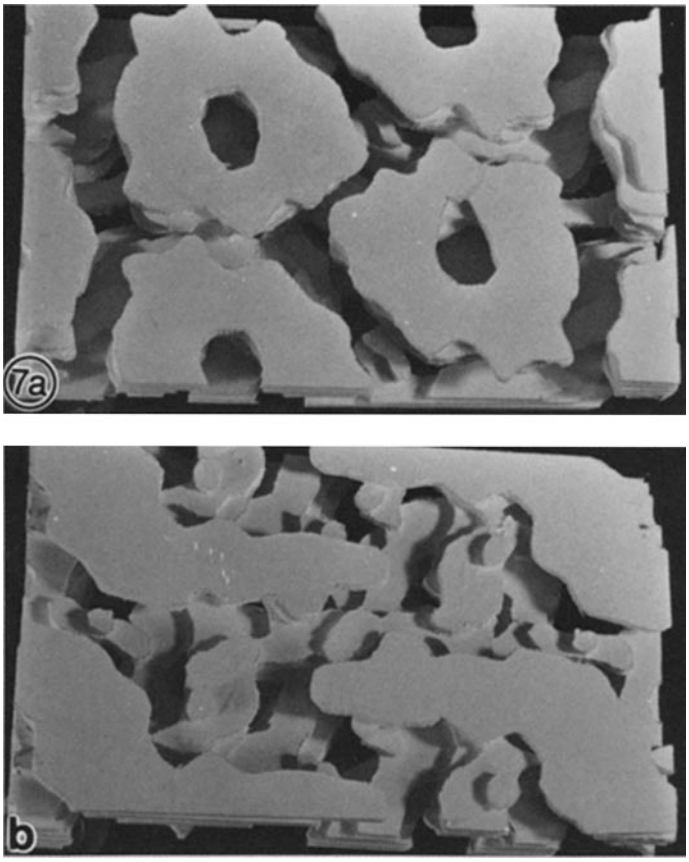

FIGURE 7 Slightly oblique views of a model derived from three-dimensional reconstruction of the crystalline membrane array at 2.5-nm resolution, viewed from the (*a*) extracellular and (*b*) intracellular side. The model represents a patch of membrane surface 37 nm by 23 nm. A double-row of particles runs vertically.

reconstruction, which causes the average density in every section parallel to the membrane to be zero. This removes therefore the variation in average density between sections at different vertical levels of the specimen. The interpretations of the reconstructed array given below are not altered by these limitations, because they depend not on averages of density over the whole section, but rather on sharp local density changes that can be reliably identified as boundaries between stain and specimen.

The reconstructed array reveals the double rows of roughly pentagonal particles to be annuli of density projecting out of the membrane into the extracellular space. Each annulus has an average outer diameter of ~11 nm and a central depression of 4-nm diam. Assuming 800 daltons/nm^3, each particle represents 5.4×10^5 daltons. The sharp boundaries of the annuli merge, and the central hole terminates abruptly, at a distance of ~2.5 nm inwards from the extracellular surface. This level presumably is the point at which stain penetration from the extracellular side is blocked by the lipid bilayer. The sample lies with its extracellular side towards the carbon support film. Stain seems to accumulate preferentially in the channels and depressions of the extracellular face, probably aided by surface forces during drying. The exposed upper intracellular face is always less well stained. It appears to have no deep channels in which stain can easily accumulate and the contrast is thus lower on this face. It is therefore difficult to determine exactly where the inner surface of the lipid bilayer should be drawn. The cytoplasmic side of the model is almost featureless, showing only a series of shallow grooves running roughly perpendicular to the rows of particles on the other surface. Since there is no information about the change in average density of the unit cell in the direction perpendicular to the membrane, one is unable to say precisely where the membrane ends and cytoplasm begins if there are no prominent protrusions to be contrasted by stain. However, taking the thickness of the bilayer in negative stain to be roughly 5 nm and its outer surface to lie at the level of the end of the holes in the extracellular projections, then the ridges would lie just inside the cytoplasm. This interpretation is consistent with the appearance of the particles in very thin sections. In Fig. 4*d*, the deep grooves between rows of particles appear to extend down to the level of the outer leaflet of the membrane lipid bilayer.

A characteristic feature of the membrane array in negative stain is the more intense staining between double rows of particles. Within each double row of particles the distribution of stain suggests a particular grouping of neighbors into pairs.

The greatest separation between particles is across the gap between double rows, and this is reflected in the mechanical properties of the membrane array. Dislocations in the array due to relative sliding between the double rows are very common, suggesting that the bonds holding the array in place are quite weak in the perpendicular direction. In contrast, dislocations within a double row have never been seen. The appearance of the array during the very early stage of disintegration in detergents reinforces this idea. The disruption begins as a splitting of the array into these double rows (Fig. 8) which themselves are more resistant to disassembly and persist after the large scale structure of the membrane complex is destroyed.

The absolute hand of the whole membrane complex was determined by tilting experiments on negatively stained "ghosts" of whole cells. In these specimens both sides of the cell are clearly seen in projection, and tilting allows one to decide which is uppermost (i.e., towards the electron source). The major features of the particle array are well visualized, since the deep grooves of the array are on the extracellular surface. The correct orientation of particle rows with respect to membrane folds was thus determined and used to orient all images relative to each other. In this way it was determined that membrane fragments nearly always lie on the grid with their extracellular face against the carbon film support. It was also determined from these ghosts that the membrane folds predominantly follow a left handed helical path around the cell, in agreement with observations by scanning electron microscopy (Fig. 1) and light microscopy.

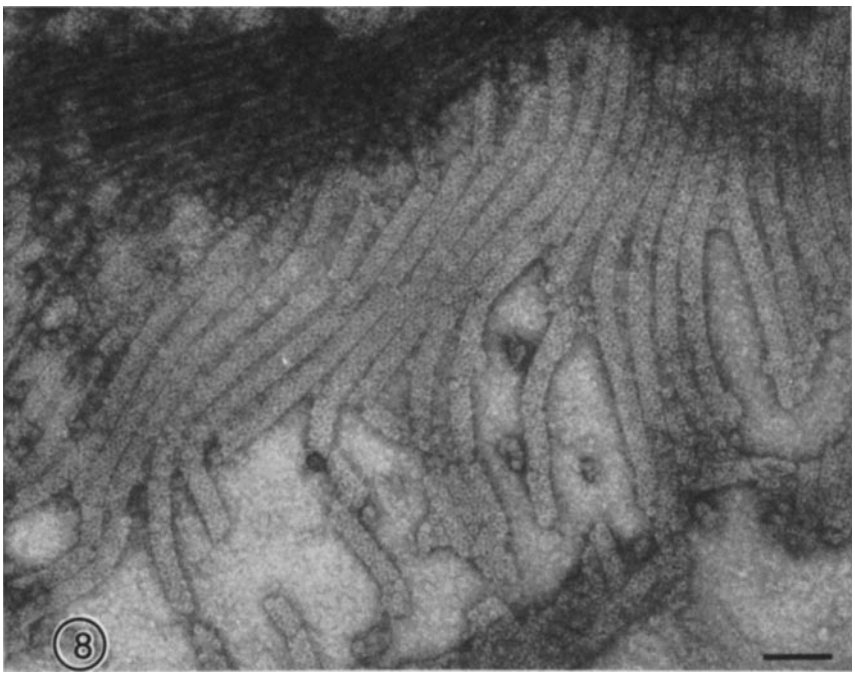

FIGURE 8 Negatively stained partially disintegrated fragment of membrane microtubule complex. Bar, 100 nm. × 92,000.

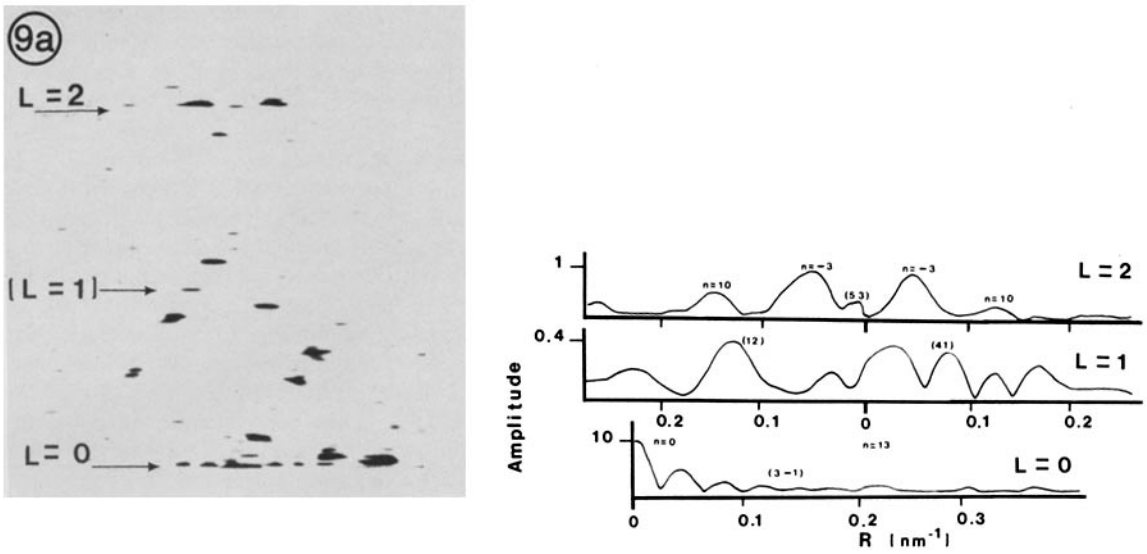

FIGURE 9 (*a*) Computed Fourier transform (top half of transform only) of a narrow strip of membrane-microtubule complex including a straight stretch of a single microtubule (middle microtubule from the group of five in Fig. 3*c*). The equator ($L = 0$) and ¼-nm^{-1} layer line ($L = 2$) are indicated, as well as the expected location of an ⅛-nm^{-1} ($L = 1$) layer line. The vertical scale is expanded by twofold relative to the horizontal in this picture. (*b*) Plot of the amplitude along each of the three microtubule layer lines in *a*. Bessel order assignments for each of the major peaks, and overlapping reflections from the membrane lattice are indicated.

Structure of the Microtubules

The structure of microtubules has been analyzed extensively using electron micrographs of negatively stained samples (27, 28), and x-ray diffraction patterns of oriented gels (29). There is broad agreement on the arrangement of tubulin monomers into 13 (in vivo) longitudinally oriented protofilaments, with an axial displacement between adjacent protofilaments of 0.92 nm (30). Lines connecting monomers with their nearest neighbors in two directions on the surface of the microtubule trace out two families of helices: a three-member left handed family and a 10-member right handed family. These contribute to the diffraction pattern as weighted Bessel function of order 3 and 10 on a line of intensity at ¼ nm^{-1} from the equator. This layer line is always the most prominent and usually the only off equatorial intensity observed in Fourier transforms of images of negatively stained microtubules.

Longer periods than the basic monomer repeat at ¼ nm^{-1} are occasionally observed in diffraction patterns of microtubules from some sources. The A tubule of the flagellar doublet microtubule gives an ⅛ nm^{-1} layer line that was interpreted as indicating a pairing of the tubulin monomers along each protofilament into dimeric units (27). Association of other proteins with microtubules, decorating the basic surface lattice on a regular subset of the total monomers, gives rise to a superlattice with probable true axial repeat of 96 nm (31).

Fig. 9*a* shows the transforms computed from a selected length of one microtubule bound to a negatively stained *Distigma* membrane complex. Intensity is contributed both from the microtubule and membrane array. A plot of amplitude along the layer line at ¼ nm^{-1}, ⅛ nm^{-1}, and on the equator is shown in Fig. 9*b*. The intensity distribution on the ¼ nm^{-1} layer line is substantially the same as has been previously observed (27, 28). The phase differences between corresponding peaks on opposite sides of the meridian indicate fairly good preservation of helical symmetry, and agree well with the reported assignments of Bessel order 3 and 10 (For $n = -3$, the phases are 280° and 70°; ideally they would differ by 180°: For $n = 10$, 270° and 280°; ideally they would be equal). The equator of Fig. 9*a* is also consistent with that observed previously, with the exception of the region affected by overlap with the (3 $\bar{1}$) membrane lattice reflection. There are 13 protofilaments in *Distigma* microtubules, (Fig. 2*c*) as in other cells. The microtubules of the membrane complex thus appear to be structurally similar to those from other eucaryotic organisms. Further evidence of similarity is provided by the ability to grow extended microtubules from the broken ends of those attached to the membrane using bovine brain tubulin (12).

In Fig. 9 and other computed transform of lengths of microtubule on the membrane complex, peaks of intensity significantly above background are always found in the region expected for a ⅛ nm^{-1} layer line. The strongest of these peaks coincide with expected membrane lattice reflections, as indicated. The phase difference between other trans-meridional pairs on this potential layer line is not consistently close to zero or 180°, suggesting that any helical information present in this region is severely contaminated by noise, or dominated by membrane lattice contributions.

The lengths of straight microtubule available on the membrane complex are too small to allow effective averaging of material repeating with long periods such as 96 nm, so no strong evidence for or against their existence can be inferred from the absence of such a layer line in Fig. 9. The overall conclusion from the Fourier transforms of negatively stained *Distigma proteus* microtubules is that they are indistinguishable at 4-nm resolution from other previously studied microtubules.

DISCUSSION

Arrangement of Microtubules on the Membrane

In principle, the microtubules could bind either directly to cytoplasmic protrusions of the membrane particle (or other

integral membrane protein) or via an intermediate bridging protein. Since the microtubules are observed to be 12 nm or so from the lipid bilayer in the thin sections, whereas the membrane particle protrude into the cytoplasm less than 5 nm in the reconstruction, a bridging protein seems necessary.

The decoration of microtubules in vitro with mixtures of high molecular weight microtubule-associated proteins (MAP)[1] changes the packing of microtubules in centrifuged pellets, and their appearance in thin sections, in a way that suggests periodic extensions from the surface of 20 to 30 nm length are formed (31, 32). A protein of this sort would be sufficiently long for binding the microtubule to the membrane complex. Regardless of the identity of the linking agent, the orderly arrangement of tubules over long distances on the membrane complex implies that the spacing between potential binding sites on the microtubule is closely matched by that of complementary sites on the cytoplasmic surface of the membrane. All of the peaks significantly above background in the Fourier transforms of negatively stained membrane complex lie on the reciprocal lattice of the membrane particle array. Thus all of the ordered structure in the membrane complex repeats with the characteristic spacing of the membrane particles. The array of membrane particles covers the entire cell surface. Therefore, any recurring microtubule binding site must fit into the same arrangement. We are thus led to expect a congruence between the observed symmetry of the membrane particle array and some regular subset of the helical surface lattice of tubulin monomers in the microtubule.

Amos (31) has investigated the distribution of MAP on brain microtubules and concluded that they are arranged on a superlattice of the basic tubulin monomer helical surface lattice. This superlattice is a one-start right-handed helix having 13 units in each repeat of 96 nm along the microtubule. A helical repeat of 96 nm is also found in diffraction patterns of whole flagella and flagellar doublet microtubules (33), suggesting that it may be a generally preferred pattern for binding of diverse proteins to microtubules.

A comparison of this probable MAP lattice with the membrane particle lattice determined in this study is shown in Fig. 10*a*. The membrane lattice is viewed from inside the cell, and the MAP lattice projection is that seen when the outside surface of the (unrolled) microtubule faces the cytoplasmic surface of the membrane. This corresponds to the view from inside the microtubule, reversed from the normal view, and thus the mirror image of Fig. 6*a* in Amos (31). A very good match occurs when the MAP arrangement is superimposed on the membrane lattice with the microtubules running at a 36° angle clockwise from the major membrane rows. The calculated membrane array unit cell that gives a perfect match has dimensions $a = 28.4$ nm, $b = 14.4$ nm, $\gamma = 95.7$, identical within experimental error to the observed valves.

Equivalent portions of the membrane array unit cell make identical contacts with every MAP molecule along one protofilament (e.g., that protofilament closest to the membrane) if the microtubules lie at a 36° angle clockwise from the membrane particle rows (Fig. 10*a*). These contacts would occur at intervals of 96 nm along a given microtubule, this being the distance between adjacent MAP bound along a single protofilament. As shown in Fig. 10*a* the MAP positions

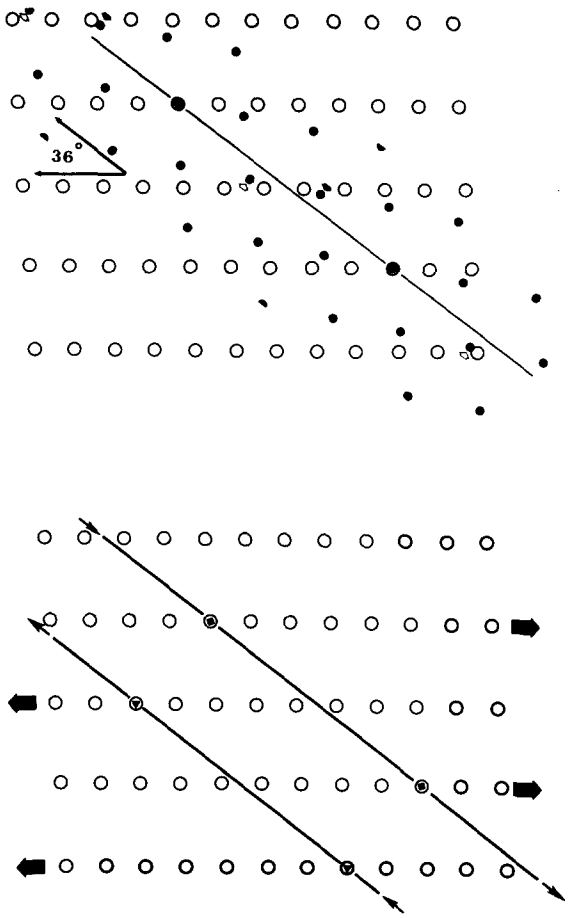

FIGURE 10 Diagram to show the correspondence between the symmetries of the membrane particle array (open circles) and the expected arrangement of MAP on microtubules (solid circles). The membrane array unit cell has dimensions 28 by 14 nm, $\gamma = 96°$. The MAP occur at intervals of 12 tubulin dimers (i.e., 96 nm). Along each of the 13 protofilaments, the MAP locations are staggered, giving rise to a helical super-lattice (31). (*top*) A short length of a single microtubule, unrolled and viewed from the inside, has been laid on a patch of membrane. Open circles represent equivalent points in each unit cell of the membrane particle array. Solid circles locate the occurrence of a MAP on the unrolled microtubule surface when they decorate the microtubule as proposed by Amos (31). When the microtubule crosses the membrane array at 36° as shown, every MAP located on one protofilament (thin line) makes identical contacts with the membrane array (concentric open and solid circles). The MAP of adjacent protofilaments on either side (the solid circles indicated by open and solid arrows) do not make the same contact. (*bottom*) Membrane array representation as in *top*. Short lengths of two microtubules are here represented by a single line each, connecting the MAP molecules along a protofilament by which each is bound to the membrane (solid squares or triangles inside circles). The microtubules do not individually restrict the rows of the membrane array in uniform sliding motions. Sliding of membrane particle rows (thick arrows) is coupled to relative longitudinal displacements of the microtubules (thin arrows).

of adjacent protofilaments within the same microtubule would not be able simultaneously to make exactly equivalent contacts with the membrane particle array.

Assuming for the moment that microtubules bind to the membrane via the MAP located on one of their protofilaments, it is of interest to determine the possible relative locations of multiple microtubules all bound in the same way.

[1] *Abbreviation used in this paper:* MAP, microtubule-associated proteins.

To simplify the description, let us denote the line joining the contacts between membrane array and MAP of a single protofilament as the "location" of the microtubule containing that protofilament (i.e., the thin line in Fig. 10*a*). With this convention, the minimum lateral separation between potential microtubule "locations" is ~4.3 nm. Of course, this means adjacent "locations" could never be simultaneously occupied, since the microtubule diameter is much greater, ~24 nm. The importance of this minimum is that the assumed binding scheme leads to a prediction: the lateral separation of microtubules bound to the membrane should always be an integral multiple of 4.3 nm. Currently, this prediction cannot be evaluated since the predicted discrete values of lateral separation would be smeared into a continuum at the present resolution. Groups of microtubules bound to the membrane with constant center to center separation would also have a constant relative axial displacement. This arrangement would lead to sampling of both the equator and ¼ nm^{-1} layer line as observed when multiple equally spaced microtubules are included in the transformed image (Fig. 6*a*).

It is also of interest to consider possible implications of the proposed binding scheme for euglenoid movement. A microtubule bound to the membrane at intervals of 96 nm along its length would be linked to alternate double-rows of membrane particles. Local sliding between these double rows therefore need not be accompanied by flexion of the microtubule (Fig. 10*b*). Thus microtubule binding may have very little effect on the flexibility of the membrane complex in small deformations. If two adjacent microtubules were bound to different sets of double rows, then sliding of double-rows would be coupled to relative longitudinal motion of one microtubule past the other. This would be one way of coupling microtubule sliding to membrane deformation with minimal change in membrane-microtubule bonding. Gross movement between double rows that produced curvature of the surface folds in the plane of the membrane would of course require flexion of the microtubules as well as sliding displacements of microtubules and sliding between adjacent double rows of particles. A more detailed analysis of the relationship of euglenoid movement to the structure reported here is currently underway.

To obtain further evidence for the hypothetical protein decorating the microtubules with the predicted helical symmetry, it will be necessary to separate microtubule from membrane complexes. A straight stretch of microtubule 5–10 μm long would be needed to obtain good averaging of a 96-nm unit cell. The residual curvature of membrane fragments is too great for them to be useful. If a way can be found to dissociate the membrane bound microtubules with retention of all MAP, then longer straight pieces may be obtained, which would permit a direct test of the predicted binding scheme.

Fig. 11 shows a short section of microtubule modeled from flattened spheres, with projections arranged on the one-start helix of 96-nm repeat as described by Amos (31), positioned beneath a model of the membrane lattice. The symmetry, orientation, and scale, are as observed. The position and shape of the projections from the microtubules is of course arbitrary, since they are not directly visualized in the reconstruction.

The shape of the particles in the membrane overlying the microtubules is found, in projection at least, to be very similar to those in adjacent areas free of microtubules. Further evidence of this similarity comes from experiments in which new

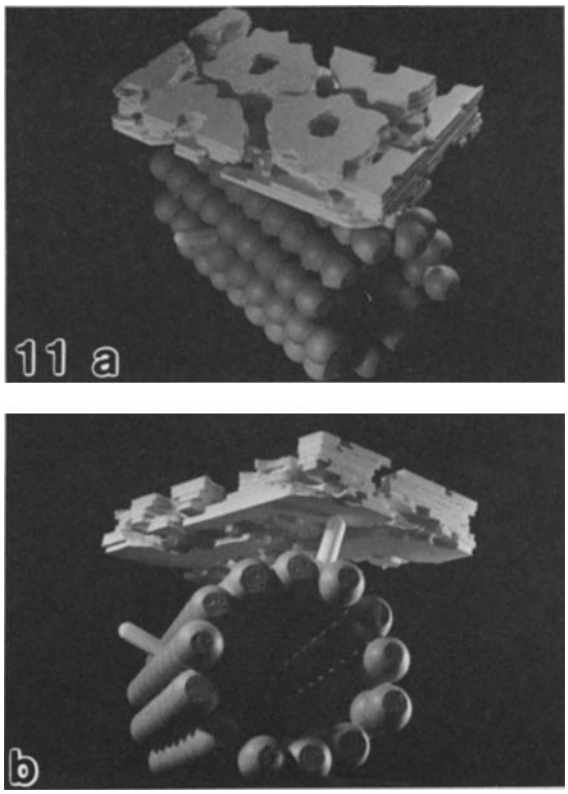

FIGURE 11 Three-dimensional model of the membrane microtubule complex from *Distigma proteus*. The views are from (*a*) slightly outside and (*b*) just underneath the cell membrane. Tubulin monomers have been approximated by flattened spheres.The projections from the microtubule represent possible proteins linking the microtubule to the cell membrane.

microtubules are bound to the membrane complex in vitro (12), with little preference for any particular area of the cytoplasmic surface. One therefore wonders why the microtubules in vivo are found in a predictable location, under only one side of the membrane fold as seen in Fig. 2*b*. No direct evidence is yet available to answer this question, but the unusual mode of cell division in these organisms suggests one possibility. Growth in *Astasia longa* (8), another of the Euglenophyceae, and in *Euglena gracilis* (25), has been shown to occur by insertion of new membrane folds between each existing fold, followed by a longitudinal fission into two daughter cells. The plane of cell division follows a helical path connecting two of the surface folds on opposite sides of the cell. Insertion of the new membrane material seems to occur starting from one edge of each old fold, with a gradual increase to the width of a fully differentiated fold. If tubulin synthesis or polymerization were linked to coincide with only one part of this cycle, and localized near the site of new membrane insertion, then the observed distribution of microtubules might result.

The true function of this remarkable microtubule membrane assembly must remain a matter for speculation at present. The most striking behavior of this class of organism is its constant rapid change of shape. A role in this movement is an attractive hypothesis for the function of the microtubules (34), but no data support it directly.

Part of this work was carried out during a postdoctoral fellowship in the laboratory of Dr. P. N. T. Unwin, whose advice and instruction

in the determination of structure by electron microscopy were invaluable. An earlier version of the manuscript was much improved by the comments of Dr. K. Nishikura and Dr. A. Weber.

Support for this work was provided in part by National Institutes of Health grant GM 30814 and GM 27764.

Received for publication 7 June 1983, and in revised form 19 August 1983.

REFERENCES

1. Smith, S., U. Järlfors, and R. Beranek. 1970. The organization of synaptic axoplasm in the lamprey (*Petromyzon marinus*) central nervous system. *J. Cell Biol.* 46:199–219.
2. Reaven, S. P., and S. G. Axline. 1973. Subplasmalemmal microfilaments and microtubules in resting and phagocytizing cultivated macrophages. *J. Cell Biol.* 59:12–27.
3. Westrum, L. E., and E. G. Gray. 1977. Microtubules associated with postsynaptic 'thickenings'. *J. Neurocytol.* 6:505–518.
4. Albertini, D. F., and J. I. Clark. 1975. Membrane-microtubule interactions: concanavalin A capping induced redistribution of cytoplasmic microtubules and colchicine binding proteins. *Proc. Natl. Acad. Sci. USA.* 72:4976–4980.
5. Weatherbee, J. A. 1981. Membranes and cell movement: interactions of membranes with proteins of the cytoskeleton. *Int. Rev. Cytol. Suppl.* 12:113–176.
6. Weihing, R. R. 1979. The cytoskeleton and plasma membrane. *Methods Achieve. Exp. Pathol.* 8:42–109.
7. Dentler, W. L. 1981. Microtubule-membrane interactions in cilia and flagella. *Int. Rev. Cytol.* 72:1–47.
8. Hofmann, C., and G. B. Bouck. 1976. Immunological and structural evidence for patterned intussusceptive surface growth in a unicellular organism. *J. Cell Biol.* 69:693–715.
9. Mignot, J. P. 1965. Ultrastructure des eugleniens. *Protistologica.* 1:5–15.
10. Sommer, J. R. 1965. The ultrastructure of the pellicle complex of *Euglena gracilis. J. Cell Biol.* 24:253–257.
11. Leedale, G. F. 1964. Pellicle structure in *Euglena. Brit. Phycol. Bull.* 2:291–306.
12. Murray, J. M. 1984. *J. Cell Biol.* In press.
13. Pringsheim, E. G. 1946. The biphasic or soil water culture method for growing algae and flagellata. *J. Ecol.* 33:193–204.
14. Spurr, A. R. 1969. A low viscosity epoxy resin embedding medium for electron microscopy. *J. Ultrastruct. Res.* 26:31–43.
15. Binder, L. I., and J. L. Rosenbaum. 1978. The in vitro assembly of flagellar outer doublet tubulin. *J. Cell Biol.* 79:500–515.
16. Mizuhira, V., and Y. Futaesaku. 1971. On the new approach of tannic acid and digitonine to the biological fixatives. *Proceedings of the Electron Microscopy Society of America.* 29:494–495.
17. Futaesaku, Y., V. Mizuhira, and H. Nakamura. 1972. The new fixation method using tannic acid for electron microscopy and some observations of biological specimens. *Proc. 4th Int. Congress of Histochem. and Cytochem., August 1972, Kyoto, Japan.* 155–156.
18. Unwin, P. N. T., and R. Henderson. 1975. Molecular structure determination by electron microscopy of unstained crystalline specimens. *J. Mol. Biol.* 94:425–440.
19. Henderson, R., and P. N. T. Unwin. 1975. Three-dimensional model of purple membrane obtained by electron microscopy. *Nature (Lond.)* 257:28–32.
20. Morrison, M. 1974. The determination of the exposed proteins on membranes by the use of lactoperoxidase. *In* Methods in Enzymology, Vol. 32B. S. Fleischer and L. Packer, editors. Academic Press, Inc., New York. 103–109.
21. Laemmli, U. K. 1970. Cleavage of structural proteins during the assembly of the head of bacteriophage T4. *Nature (Lond.).* 227:680–685.
22. Bürk, R. R., M. Eschenbruch, P. Leuthard, and G. Steck. 1983. Sensitive detection of proteins and peptides in polyacrylamide gels after formaldehyde fixation. *In* Methods in Enzymology. C. H. W. Hirs and S. N. Timasheff, editors. Academic Press, Inc., New York. 91:247–254.
23. Heidemann, S. R., and J. R. McIntosh. 1980. Visualization of the structural polarity of microtubules. *Nature (Lond.).* 286:517–519.
24. Miller, K. R., and G. J. Miller. 1978. Organization of the cell membrane in *Euglena. Protoplasma.* 95:11–24.
25. Lefort-Tran, M., M. H. Bre, J. L. Ranck, and M. Pouphile. 1980. *Euglena* plasma membrane during normal and vitamin B_{12} starvation growth. *J. Cell Sci.* 41:245–261.
26. DeRosier, D. J., and A. Klug. 1968. Reconstruction of three-dimensional structures from electron micrographs. *Nature (Lond.).* 217:130–134.
27. Amos, L. A., and A. Klug. 1974. Arrangement of subunits in flagellar microtubules. *J. Cell Sci.* 14:523–549.
28. Erickson, H. P. 1974. Microtubule surface lattice and subunit structure and observations on reassembly. *J. Cell Biol.* 60:153–167.
29. Cohen, C., D. DeRosier, S. C. Harrison, R. E. Stephens, and J. Thomas. 1975. X-ray patterns from microtubules. *Ann. N. Y. Acad. Sci.* 253:53–59.
30. Linck, R. W. 1982. Structure of microtubules. *Ann. N. Y. Acad. Sci.* 383:98–121.
31. Amos, L. A. 1977. Arrangement of high molecular weight associated proteins on purified mammalian brain microtubules. *J. Cell Biol.* 72:642–654.
32. Kim, H., L. I. Binder, and J. L. Rosenbaum. 1979. The periodic association of MAP2 with brain microtubules in vitro. *J. Cell Biol.* 80:266–276.
33. Amos, L. A., R. W. Linck, and A. Klug. 1976. Molecular structure of flagellar microtubules. *In* Cell Motility. R. Goldman, T. Pollard, and J. Rosenbaum, editors. Cold Spring Harbor Laboratory, Cold Spring Harbor, New York. 847–867.
34. Murray, J. M. 1981. Control of cell shape by calcium in the Euglenophyceae. *J. Cell Sci.* 49:99–117.